Relative Microelastic Mapping of Living Cells by Atomic Force Microscopy

Emad A-Hassan,* William F. Heinz,* Matthew D. Antonik,* Neill P. D'Costa,* Soni Nageswaran,* Cora-Ann Schoenenberger,# and Jan H. Hoh*

*Department of Physiology, Johns Hopkins University School of Medicine, Baltimore, Maryland 21205 USA and #Müller Institute for Microscopy, Biozentrum, University of Basel, Basel CH-4056, Switzerland

ABSTRACT The spatial and temporal changes of the mechanical properties of living cells reflect complex underlying physiological processes. Following these changes should provide valuable insight into the biological importance of cellular mechanics and their regulation. The tip of an atomic force microscope (AFM) can be used to indent soft samples, and the force versus indentation measurement provides information about the local viscoelasticity. By collecting force-distance curves on a time scale where viscous contributions are small, the forces measured are dominated by the elastic properties of the sample. We have developed an experimental approach, using atomic force microscopy, called force integration to equal limits (FIEL) mapping, to produce robust, internally quantitative maps of relative elasticity. FIEL mapping has the advantage of essentially being independent of the tip-sample contact point and the cantilever spring constant. FIEL maps of living Madine-Darby canine kidney (MDCK) cells show that elasticity is uncoupled from topography and reveal a number of unexpected features. These results present a mode of high-resolution visualization in which the contrast is based on the mechanical properties of the sample.

INTRODUCTION

The structure of eukaryotic cells is controlled by a dynamic balance of mechanical forces. Intrinsic properties of the molecular components and the actively generated forces, such as the forces exerted by the cytoskeleton on the extracellular matrix (ECM) attachments, neighboring cells, and the substratum contribute to this force balance (Ingber et al., 1994; Li et al., 1987). When it is altered, integrated changes in cell form, cytoskeletal organization, and nuclear shape result. Growth, cell cycle progression, gene expression, and other cell behaviors are sensitive to changes in the cellular mechanical force balance or closely associated changes in the cytoskeleton, ECM mechanics, and nuclear structure (Ingber, 1993; Ingber et al., 1995; Mooney et al., 1992; Singhvi et al., 1994; Mitchison, 1995). Hence, spatial and temporal modulations of cellular mechanical properties are intimately related to physiologically important processes. For instance, changes in local mechanical properties are thought to be vital for tissue pattern development, especially during embryonic morphogenesis (Fung, 1988; Ingber and Folkman, 1989; Ingber and Jamieson, 1985). Modulation of the tension-dependent cell shape is central to the process by which angiogenesis is regulated (Ingber et al., 1995). Neurons also undergo growth and morphogenetic changes in response to mechanical tension (Zheng et al., 1991). Measurements of the spatial distribution and changes in viscoelastic properties of living cells will provide valuable insights into these processes.

The mechanical properties of cells have been studied with various techniques. Among these methods, the cell poker was used to study cellular deformability based on the resistance of a cell to indentation with a flat-ended glass fiber (Peterson et al., 1982; Zahalak et al., 1990). Other techniques include the micropipette aspiration (Young and Evans, 1989; Shao and Hochmuth, 1996), flicker or dynamic reflection interference contrast spectroscopy (Zilker et al., 1987; Zeman et al., 1990), scanning acoustic microscopy (Luers et al., 1991; Bereiter-Hahn et al., 1995), infrared laser traps (optical tweezers) (Ashkin and Dziedzic, 1989; Svoboda et al., 1992), and various magnetometric analysis devices that use magnetic particles bound to extracellular receptors or introduced into intact living cells (Valberg and Feldman, 1987; Wang and Ingber, 1994; Maniotis et al., 1997). Most of these methods, however, average properties over relatively large areas and hence have very modest spatial resolution.

The atomic force microscope (AFM; Binnig et al., 1986) is emerging as a valuable tool for studying biological materials (Kasas et al., 1997; Hansma and Hoh, 1994; Henderson, 1994). It is well established that the AFM can be used to image living cells under physiological conditions in a nondestructive manner (Schaus and Henderson, 1997; Schoenenberger and Hoh, 1994; Butt et al., 1991; Henderson et al., 1992; Hoh and Schoenenberger, 1994; Haydon et al., 1996). The AFM can also be used to study material properties by collecting so-called force curves over a point on the sample surface (for a review see Bottomley et al., 1996). A force curve is a plot of the force applied to the AFM tip as the sample is approached and pushed against the tip. In principle, this plot gives the force required to achieve

Received for publication 4 August 1997 and in final form 20 November 1997.

Address reprint requests to Jan H. Hoh, Department of Physiology, Johns Hopkins University School of Medicine, 725 N. Wolfe Street, Baltimore, MD 21205. Tel.: 410-614-3795; Fax: 410-614-3797; E-mail: jan.hoh@jhu.edu.

0006-3495/98/03/1564/15 $2.00

a certain depth of indentation (deformation) from which viscoelastic parameters can be determined. For biological materials, the AFM force curves have been used to examine micromechanical properties of bones (Tao et al., 1992), platelets (Radmacher et al., 1996), magnetotactic bacteria (Fritz et al., 1994), atrial myocytes (Shroff et al., 1995), embryonic carcinoma cells (Goldmann and Ezzell, 1996), glial cells (Haydon et al., 1996), epithelial cells (Putman et al., 1994; Hoh and Schoenenberger, 1994), and cholinergic synaptic vesicles (Laney et al., 1997). By collecting arrays of force curves, so-called force volumes, high-resolution 2-D maps of mechanical properties can be produced.

Despite these demonstrations of the utility of micromechanical mapping with the AFM, there are several experimental difficulties in collecting and quantitatively analyzing the force curve data. One of the most vexing problems is accurate determination of the contact point between the tip and the sample. If a sample is soft relative to the detection sensitivity of the AFM, the sample will deform in response to the tip before the cantilever deflects measurably and the true contact point is not easily detected. Large uncertainty in the contact point leads to significant errors in the estimation of the indentation depth, elastic moduli, or any other parameter defined by the contact point. In particular, errors occur when the force curve data are fitted to the commonly used Hertz model (Weisenhorn et al., 1992; Radmacher et al., 1995, 1996). The determination of a Young's modulus also requires accurate force measurement, which makes calibration of the AFM cantilever an additional essential parameter. However, cantilever calibration is relatively cumbersome and time consuming with many potential sources of errors. Finally, the wide range of AFM tip shapes and the small tip-sample contact area make the contact geometry poorly defined.

These problems have motivated us to develop a set of experimental conditions and a new analytical approach for analyzing AFM force curves to produce robust and internally quantitative micromechanical maps. In this report we describe this new approach and its application on Madine-Darby canine kidney (MDCK) cells. MDCK cells are a well-characterized epithelial cell system (Matlin and Caplan, 1992; Balkovetz et al., 1997) that forms continuous monolayers. MDCK cells serve as a suitable model system to develop and demonstrate this new approach to mapping the relative microelastic properties of living cells with high spatial resolution.

FIEL MAPPING

To deal with the experimental difficulties described above we have developed a new analytical framework for determining relative microelastic properties from force volumes of viscoelastic materials, called FIEL (force integration to equal limits). FIEL mapping has the advantages of being independent of the tip-sample contact point, not requiring calibration of the AFM cantilever force constant, and reducing differences in probe geometry to a simple geometric scaling factor. It should be noted that the emphasis of FIEL mapping is to show differences and changes in local viscoelastic properties. The following section describes the experimental conditions and theoretical basis of FIEL mapping.

Force-distance and force-time curves

AFM force curves are collected by measuring the cantilever deflection (d_c) as the sample is moved toward the tip. Fig. 1 *A* shows a typical approaching force curve collected on an MDCK monolayer as a plot of the change in cantilever deflection (Δd_c) versus the height position of the sample (ΔZ_p). This curve is collected in relative trigger mode (RT-mode) in which the sample is advanced until a preset cantilever deflection relative to the zero deflection position is reached. The sample is then retracted a predetermined distance. On a hard nondeformable surface, Δd_c is proportional to ΔZ_p while the tip and the sample are in contact. However, soft samples deform with increasing cantilever deflection, resulting in a nonlinear contact region of the curve. This curve is a convolution of the viscoelastic properties of the sample with the viscoelastic properties of the cantilever.

Rather than using sample position (Z_p), it is more useful to use an absolute distance (D) that is relative to the separation between the tip and the sample surface (for a soft sample this is the undeformed surface). The correction to produce a force-distance (FD) curve uses the relationship $D = \Delta Z_p - \Delta d_c$ (Ducker et al., 1992; Butt et al., 1995) (Fig. 1 *B*). Because force and deflection are directly related through Hooke's Law, $F_c = k_c \cdot \Delta d_c$, where F_c is the force on the cantilever and k_c is the force constant of the cantilever; the word force is often used here to describe cantilever deflections even in the absence of measured k_c. Note that it is essential to calibrate the optical lever sensitivity before every force measurement for accurate conversion of the photo diode response to cantilever deflection (D'Costa and Hoh, 1995).

The FIEL theory described below requires that the force curve data are dominated by the elasticity of the sample and that the contribution of viscosity is minimized. To examine the relationship between elastic and viscous contributions we have used force-time (FT) curves that show the time-dependent relaxation of a viscoelastic sample in response to an applied force (Fig. 1 *C*). In FT curves the tip is initially (period A-B in Fig. 1 *C*) not in contact with the cell, and the cantilever deflection signal is constant (zero). At point B, a step voltage is applied to the piezo giving a rapid upward displacement in the z-direction only. Due to the viscosity of the fluid surrounding the sample, the tip will initially deflect to point C. The magnitude of that deflection will depend on the step size, step rate, distance between the tip and the sample before contact with the sample's surface, and the viscosity of the fluid. The cantilever very rapidly relaxes to point D, which is in contact with the sample; note that the

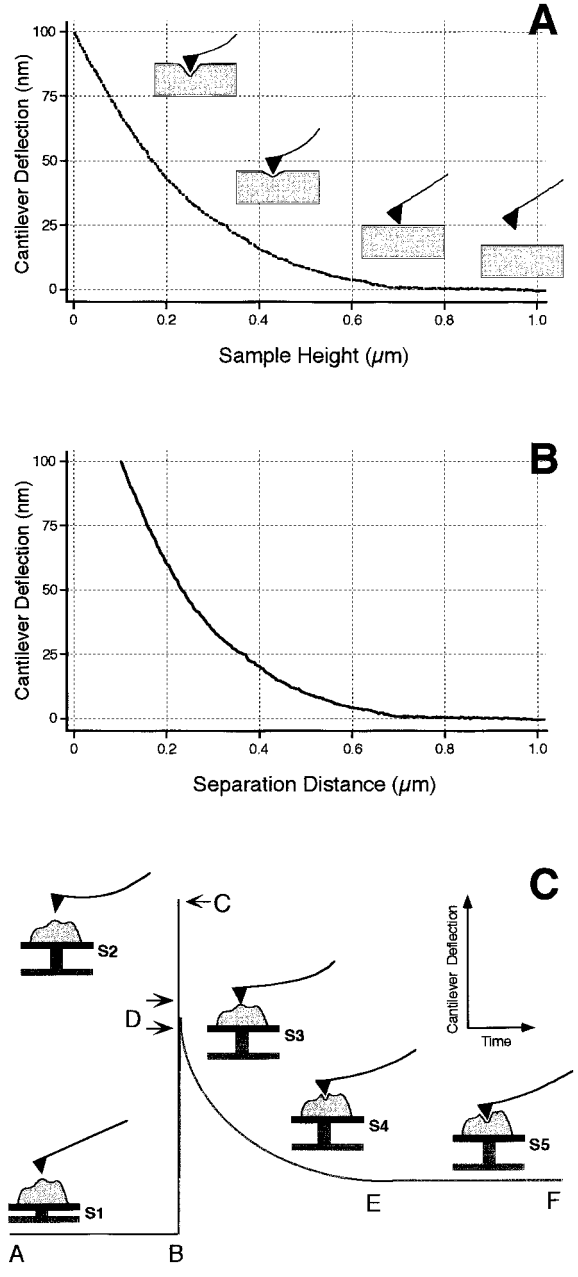

FIGURE 1 (*A*) The approaching (extending) trace of a force curve collected on an MDCK monolayer. The schematic drawings depict the relative positions of the AFM tip and the sample surface as related to the force curve. The horizontal axis shows the distance over which the piezo has been moved and the vertical axis records the change in photodiode output (which is proportional to the cantilever deflection). The nonlinear response of the cantilever in the contact region is a result of the sample indentation and cantilever deflection. (*B*) The corresponding force versus tip-sample separation distance (FD) curve. (*C*) Schematic for the time-dependent relaxation measurements (FT curves). The figure shows the position of the cantilever as a function of time. During period [A-B], (s1), the tip is not in contact with the cell and the cantilever deflection is constant. At point B, a step voltage is applied to the piezo resulting in an upward displacement of the sample. Due to movement of the sample and the hydrodynamic drag, the cantilever will deflect to point C (s2) before coming in contact with the cell surface (s3) in the interval marked by D. The cell deforms due primarily to cellular viscosity (s4), during the period after point D, to a new equilibrium (s5), period [E-F], where elastic properties dominate.

contact point D is ill-defined. The time required for the sample to deform in response to the applied force, during the period after point D, is related to the viscosity of the sample. The new equilibrium position of the cantilever is predominantly due to the elastic properties. This separation of viscous and elastic contributions based on time dependence is of course not complete, but is an adequate approximation at the present time. We further assume that there are no deformations that are effectively plastic, which will be shown below to be true for small deformations.

Collecting arrays of force curves to produce microelastic maps typically requires at least 1024 curves (32 × 32) for producing a map with reasonable resolution and identifiable morphology. The large number of curves requires that each curve is collected as quickly as possible in order to produce a map in the least time possible. The FT curves yield what is most often the limiting factor to collecting force curves quickly; i.e., the separation of elasticity and viscosity. If scan rates that coincide with period (period D-E in Fig. 1 *C*) are used, the contribution of the viscous properties of the cells to the FD curve is significant. However, slower scan rates coinciding with the period [E-F] minimize the viscous contribution. Hence, it is important to consider the relaxation time constant in determining the appropriate scan parameters. In particular, the scan parameters should be such that force curves are collected on the time scale many times larger than the relaxation time constant.

The Hertz model

The Hertz model (Hertz, 1881; Johnson, 1985) describes the simple case of elastic deformation of two perfectly homogeneous smooth surfaces touching under load. The model, which has been widely applied to AFM data, describes the relationship between the contact radius, the applied load, and the central displacement for isotropic or transversely isotropic linear elastic bodies (Weisenhorn et al., 1992; Radmacher et al., 1995). If the tip of an AFM is approximated by a sphere, then the force on the cantilever (F) is given by

$$F_c = \frac{4E\sqrt{R}}{3(1-\nu)}\,\delta^{3/2}, \tag{1}$$

where δ is the indentation, E is the elastic modulus, ν is the Poisson ratio, and R is the radius of the probe sphere (Radmacher et al., 1995). Although living cells do not meet the assumptions of the Hertz model (in particular they are not isotropic), this model is likely to be adequate for a large number of applications in which absolute elasticity values are not required. One difficulty in using the Hertz model is that only two or three (force, indentation depth, and sometimes radius of the probe) of the five variables are typically measured in an AFM experiment. One value that is not available, or easily measured for living cells, is the Poisson ratio. In order to determine an elastic modulus, the Poisson ratio is typically given a value of 0.5, although this has not

been measured for living cells and is likely to vary across the surface of a cell. In addition, it is not clear how useful a quantity of an elastic modulus of a living cell is. These concerns have led us to use an elastic constant k_s, where

$$k_s = \frac{1 - \nu}{\pi E} \tag{2}$$

represents local elasticity of the sample. The use of k_s has the advantage that it allows for an indeterminate and varying (in *x, y*) Poisson ratio. It is also suitable for determining relative elasticity. We still assume that the Poisson ratio is uniform in Z over small deformations. Also, the sample is assumed to be much softer than the cantilever's tip (Si_3N_4 tip with $E_{tip} = 150$ GPa) and the k_{tip} can be neglected.

FIEL theory

To allow for comparison of the elastic properties at different positions and times we have derived a simple relationship that relates the work done by the AFM cantilever during an indentation to the k_s, which is FIEL. In FIEL mapping a pair of FD curves is collected at positions P_1 and P_2 using the relative trigger mode. Thus, imposing the condition $F_1 = F_2$ at these positions results in

$$\frac{4}{3}\frac{\sqrt{R}}{\pi k_1}\delta_1^{3/2} = \frac{4}{3}\frac{\sqrt{R}}{\pi k_2}\delta_2^{3/2}, \tag{3}$$

which reduces to

$$\left(\frac{\delta_1}{\delta_2}\right)^{3/2} = \frac{k_1}{k_2}. \tag{4}$$

The area under an FD curve is the work done by the cantilever at each position and is given by

$$w_1 = \int_o^{\delta_1} \frac{4}{3}\frac{\sqrt{R}}{\pi k_1}\delta^{3/2}\, d\delta = \frac{8}{15}\frac{\sqrt{R}}{\pi k_1}\delta_1^{5/2}, \tag{5}$$

and

$$w_2 = \int_o^{\delta_2} \frac{4}{3}\frac{\sqrt{R}}{\pi k_2}\delta^{3/2}\, d\delta = \frac{8}{15}\frac{\sqrt{R}}{\pi k_2}\delta_2^{5/2}. \tag{6}$$

Thus, the relative work (w_1/w_2), or the relative areas under the two force curves, is

$$\frac{w_1}{w_2} = \left(\frac{\delta_1}{\delta_2}\right)^{5/2}\frac{k_2}{k_1}. \tag{7}$$

From Eq. 4

$$\left(\frac{\delta_1}{\delta_2}\right)^{5/2} = \left(\frac{k_1}{k_2}\right)^{5/3}, \tag{8}$$

substituting into Eq. 7, we obtain

$$\frac{w_1}{w_2} = \left(\frac{k_1}{k_2}\right)^{2/3}, \tag{9}$$

which directly relates the area under the two force curves to the ratio of the elastic constants at P_1 and P_2. This approach also holds for other tip geometries with only a change in the scaling exponential (Table 1).

This analytical approach has several important features. It is independent of the exact probe size as long as the same probe is used in both measurements. It is also independent of the sample topography and the sample drift (in Z), and does not require absolute Z_p measurements. Furthermore, it is independent of the cantilever spring constant and cantilever deflection drift (between individual FD curves). Finally, and most importantly, it is essentially independent of the tip-sample contact point. To illustrate the latter point, Fig. 2 *A* shows a typical FD curve on an MDCK cell. As described earlier, there are three main regions of this curve; the noncontact region (a-b), the contact point (anywhere in b-c), and the contact region (c-d). Moving the contact point in or around (b-c) results in very small changes in the area.

MATERIALS AND METHODS

Cell culture

Maintenance of cell culture and preparation of cell samples for AFM imaging was done as described earlier (Hoh and Schoenenberger, 1994). Briefly, MDCK strain II epithelial cells were grown in Dulbecco's modified Eagle's medium (DMEM, GIBCO, BRL, Life Technologies, Gaithersburg, MD) containing 5% fetal bovine serum, 5 mM HEPES, and 1% penicillin/streptomycin, at 37°C and 5% CO_2, in a humidified incubator. All cultures were fed 3 times a week with fresh medium. Confluent cells were released from culture flasks and passaged every 4 weeks using trypsin-EDTA (GIBCO BRL). Cultures were discarded after 15 passages.

Sample preparation and AFM imaging

For AFM mounting, round (15 mm) glass coverslips (Ted Pella, Inc., Redding, CA) were glued with epoxy onto magnetic steel stubs of the same size, rinsed with ethanol, and autoclaved. The sterilized stubs were placed in tissue culture dishes. Confluent MDCK cells growing in plastic flasks were trypsinized and the cell suspension ($\sim 1.6 \times 10^6$ cell/ml) was plated on the mounted coverslips (~ 150 μl/coverslip). Cells were allowed to attach for ~ 2 h in the incubator before adding medium to the culture dish.

TABLE 1 Comparison of loading force and relative area for several tip geometries

Geometry	Loading Force	Relative Area
Sphere, Parabolic	$F_{sphere} = \frac{4}{3}\frac{\sqrt{R}}{\pi k}\delta^{3/2}$	$\frac{w_1}{w_2} = \left(\frac{k_1}{k_2}\right)^{2/3}$
Conical	$F_{cone} = \frac{1}{2}\frac{\tan(\alpha)}{k}\delta^2$	$\frac{w_1}{w_2} = \left(\frac{k_1}{k_2}\right)^{1/2}$
Flat-end Cylinder	$F_{cylinder} = \frac{2R}{\pi k}\delta$	$\frac{w_1}{w_2} = \left(\frac{k_1}{k_2}\right)$

*

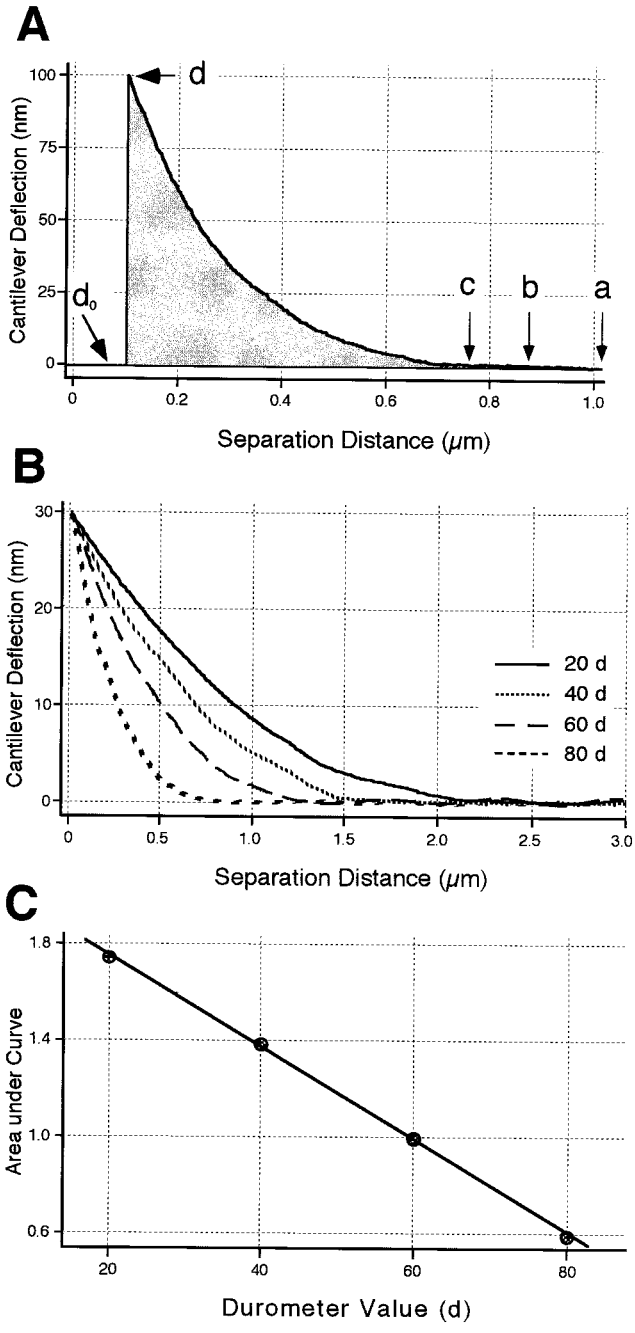

FIGURE 2 FIEL silicone polymer sheeting standards. (*A*) The work done by the cantilever is directly proportional to the area, shown in gray, under the FD curve. This is the area bounded by the zero deflection line (d_o) and d at the trigger threshold. The noncontact region (a–b), the contact point (anywhere in b-c) and the contact region (c-d) are denoted by their corresponding arrows. (*B*) FD curves for each of four different silicone standards and (*C*) the relationship between the FIEL area and the Durometer values for the standards is linear over the range of stiffness used.

Four days after plating, MDCK cells had reached saturation on the coverslips and were used for imaging and force mapping. All measurements were done within 2–3 weeks of plating.

AFM imaging was performed on a Nanoscope III atomic force microscope (Digital Instruments Inc., Santa Barbara, CA) equipped with a J-type scanner (maximum XY scan range of 150 × 150 nm with 5 μm vertical range). Silicon nitride cantilevers used (Park Scientific Instruments, Sunnyvale, CA) were either 220 × 22 μm with an estimated force constant of ~0.03 N/m or 180 × 18 μm with a nominal force constant of ~0.05 N/m. Imaging of cells was performed using a standard fluid cell without the o-ring in 1 × Hanks' balanced salt solution (GIBCO BRL) at room temperature or 37°C. For work at 37°C the AFM was placed in a warm room and allowed to equilibrate for many hours before use. Parameters were essentially as described previously by Hoh and Schoenenberger (1994). Before force mapping, images of cells were taken with a low imaging force (2–5 nN) and 1–4 Hz lateral frequency. For comparison, images were again taken after the completion of force mapping data acquisition. All forces reported are estimates based on the nominal spring constant values.

Time-dependent relaxation curves

The change in cantilever deflection (Δd_c) and the piezo-voltage (ΔZ_p) around designated set points (d_o and Z_o) were recorded using a breakout box and a LabVIEW driven data acquisition system (National Instruments, Austin, TX) as the sample was moved vertically with the scan size set to zero. The piezo Z position was controlled by custom-built electronics such that the applied voltage moves the piezo a defined distance in the Z direction. The step voltage used for relaxation measurements had a rise time of 15 μs. Analog d_c and Z_p signals were recorded at 0.1–0.5 MHz sampling rates. Measurements were done with a standard silicon nitride tip or 10 μm in diameter polystyrene sphere attached to the end of a cantilever.

Force volumes

Acquisition of force volume data sets, or force mapping, is supported by current versions of the Nanoscope control software (4.23 b6 or higher). Force mapping involves the collection of force curves extending and retracting curves) at each point in a two-dimensional (X-Y) scan. All measurements were done in relative trigger mode; i.e., all force plots have the same maximum cantilever deflection. This is done by moving the piezo vertically until the cantilever deflection has reached the trigger value: the preset maximum force. Data acquisition for the extending trace of the force curve is terminated at this point while that of the retracting trace is started. The piezo's position at that deflection is recorded as the height at that position on the sample. This height image will be referred to as the force mapping height. It is not a true height image since it is recorded at arbitrary loading forces, which can cause variable and significant deformation of cells. The piezo is then retracted an amount equal to the vertical (Z) scan size giving the retracting trace of the curve. This process is then repeated for each point in the 2-D (X-Y) scan of the sample. It is essential that the Z-scan size be large enough to pull the tip completely off the sample, but as small as possible to achieve best vertical force curve resolution. Most of our measurements were 64 × 64 force curves over the 2-D scan and each force curve (extended and retracted) had 64 points per curve, which is an upper limit imposed by the current AFM control software. Some measurements were 32 × 32 force plots and 256 points per curve, in order to obtain a high vertical resolution in the force curves.

Silicone standards

Silicone polymer sheets of known stiffness were obtained from Specialty Manufacturing Inc. (Saginaw, MI). The sheets had "Durometer" hardness test (Shore A) values of 20d, 40d, 60d, and 80d, as determined by the manufacturer. Force curves on the silicon standards were collected using standard single crystal silicone cantilevers with nominal spring constants in the range of 10–100 N/m (TESP; Digital Instruments Inc., Santa Barbara, CA).

Analysis software

Analysis and display of force mapping measurements were done with a set of tools developed in our laboratory using the Interactive Data Language

(IDL, Research Systems, Inc., Boulder, CO) programming environment, called IDEAS (Image and Data Exploration and Analysis for SPM). The FIEL mapping approach has been automated in IDEAS. Corrections to produce FD curves use the measured cantilever sensitivity in the parameter file, and FIEL values are determined by simple numerical integration. The computations for a 4096 set of force curves take <60 s on a 225 MHz Macintosh-compatible computer. The values are then scaled to a suitable color table, such that darker areas are more stiff, and displayed as a 2-D map of relative elastic constants. The maps are not corrected for specific tip geometry unless noted, and hence the relative intensities are not linearly related to the elastic constants.

RESULTS AND DISCUSSION

FIEL on standards

To test the validity of the FIEL approach, we examined silicone polymer sheets of known mechanical properties as defined by the Durometer hardness test. This test is an international standard for assessing elastic moduli of rubber and other elastomeric polymers, with low Young's moduli as compared to ceramics (Briscoe and Sebastian, 1993). The test uses an indenter, spherical or truncated cone in shape, to examine the compliance behavior of elastic materials and relates the hardness to the materials' elastic and viscous properties (Casa et al., 1995).

The custom-made silicon sheets used had durometer values of 20d, 40d, 60d, and 80d. Over this range, the theoretical, as described by the Hertz analysis of indentation, and the experimental relationship between the hardness number and the Young's modulus has been determined (Briscoe and Sebastian, 1993). Fig. 2 *B* shows FD taken over these four standards with the AFM silicon tip as the indenter probe. By integrating under the FD curve for each sample, we obtain the area, or the work done by the cantilever. Averaging the area for several measurements on a sample and plotting it against the durometer value, we obtain a linear relationship with the Durometer value (Fig. 2 *C*). Therefore, the FIEL approach is in good agreement with a commonly used measure of polymer elasticity.

Relaxation times of MDCK cells from FT curves

FT curves showing the time-dependent relaxation of MDCK cells were collected at 37°C and at room temperature (Fig. 3 *A*) to identify viscous contributions. These FT curves show a smooth and reproducible relaxation with time. Upon initial application of stress by the AFM tip there is an instantaneous deflection of the cantilever after which the tip continues to deform the cell due to the viscous (time-dependent) element. The applied force, following the viscous relaxation, is supported by the elastic element of the cell (E-F in Fig. 1 *C*).

The FT curves show relaxation times that are in the range of hundreds of milliseconds for the sharp silicon nitride tip at 37°C to a few seconds for measurements at room temperature (Fig. 3 *A*); with the time constants ($t_{1/2}$) 1–3 orders of magnitude larger at 22°C than at 37°C. There is also a dependence on probe geometry, as would be expected: i.e., larger probes producing longer relaxation times, in the tens of seconds for a 10-μm sphere (results not shown). These results show that force curves collected at 37°C, with a sharp pyramidal tip at >500 ms will be dominated by an elastic response, while at room temperature the collection time should be >10 s. In practice, these times correspond to scan rates of 10 μm/s and 0.5 μm/s. The relaxation curves

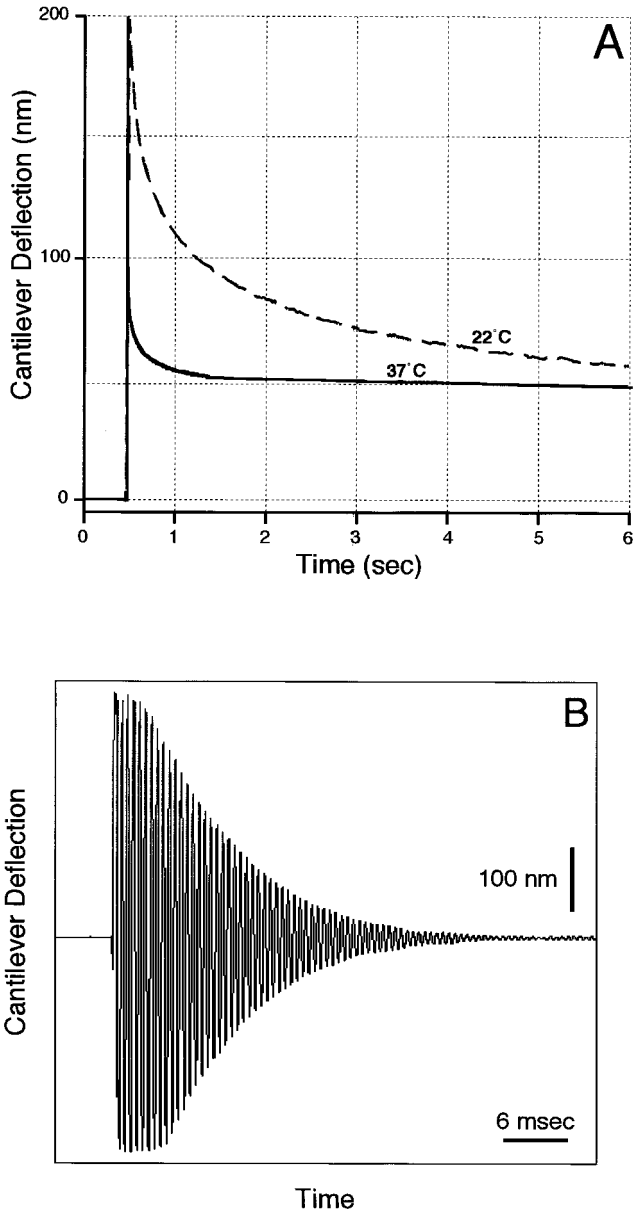

FIGURE 3 FT curves on MDCK monolayers using silicon nitride tips, produced by rapidly pressing the tip against the monolayer and recording the cantilever deflection with time. (*A*) At room temperature the cell relaxes in response to the AFM tip such that the curve becomes asymptotic in several seconds, while at 37°C it takes only several hundred milliseconds. This shows a very strong temperature dependence of the time dependent (viscous) response of living cells to an applied stress. (*B*) The initial deflection of the cantilever after the piezo step results in a hydrodynamic movement of the cantilever. This is seen here by stepping the sample without making contact, and recording the deflection, oscillation, and damping of the cantilever.

warrant a more detailed study in their own right, but the data presented here serve to demonstrate conditions that minimize the viscous contribution to the FD measurements.

A close examination of the extremely fast early relaxation of the FT curve suggests that it results from hydrodynamic drag on the cantilever during the rapid Z step. The deflection of the cantilever in response to the Z step is immediately followed by a characteristic oscillation coupled with a rapid damping. This oscillation and rapid damping can be reproduced by the Z step in the absence of contact to a surface (Fig. 3 *B*). Therefore, the instantaneous deflection value contains a large hydrodynamic component and is not useful for characterizing the cells.

FD Curves on MDCK cells

Individual force curves on MDCK cells are distinctly nonlinear, as expected for viscoelastic materials. In this section we describe the behavior of individual curves under a variety of conditions including different scan rates and indentation depths. We also examine the effect of repeated force curve collection at one position and demonstrate heterogeneity in force curves across the surface of a cell.

Force curves on living cells are known to exhibit hysteresis between the approaching and retracting curves, which is partly due to viscous effects (Hoh and Schoenenberger, 1994). Consistent with a viscous contribution, increasing the scan rate from 4 to 80 μm/s significantly increases the hysteresis to the point where at very high scan rates there is a negative deflection of the cantilever (Fig. 4). There are two separate effects that contribute to the shape of these curves. The large separation of the curves in their noncontact regions is due to the hydrodynamic drag on the cantilever (Hoh and Engel, 1993), while the hysteresis in the contact region is the result of substantial viscous contributions from the cells. The negative deflection at high scan rates has previously been reported (Hoh and Schoenenberger, 1994), but is not understood.

Repeated force curves were taken at the same position on a MDCK monolayer to examine the reproducibility of the curves. Nonreproducibility indicates plastic deformation or other effects that are not reversible on the time scale of the measurement (Fig. 5). The results show that the curves are highly reproducible at low scan rates (5–25 μm/s), while at higher scan rates some variation between curves begins to appear. This further supports the notion that elastic mapping should be performed at relatively low scan rates.

To determine the effect of an increase in the maximal force applied we collected a series of FD curves over a single position on an MDCK monolayer with increasing trigger threshold (Fig. 6). These FD curves are aligned by their maximum deflection values. The curves are in good agreement at the two smaller deflections of 25 and 50 nm, while a small deviation at the 100-nm deflection threshold, and a significant one at the 200-nm deflection, are observed. This suggests that there is a deformation for the larger

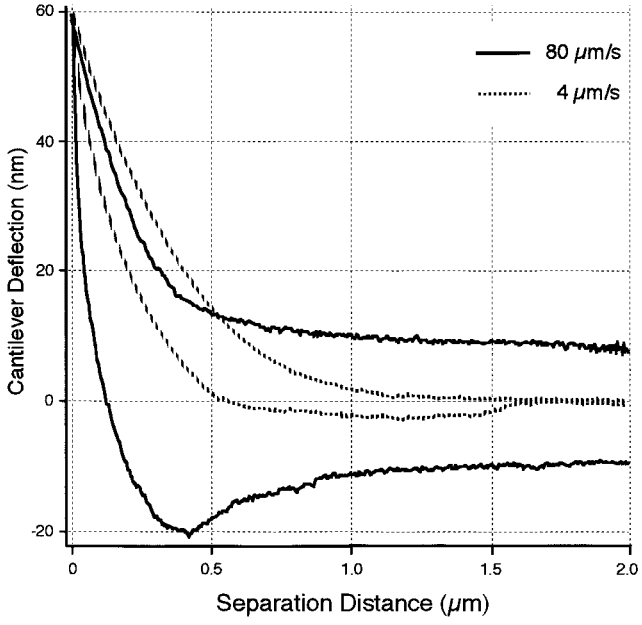

FIGURE 4 FD curves taken over the same point on an MDCK monolayer at different scan rates (the top curves in each pair are the approaching trace, and the lower are the retracting trace). Due to hydrodynamic drag, there is an increase in separation of noncontact parts of the approach and retract curves as the scan rate is increased. At low Z scan rates, a hysteresis in the contact region can be seen between the approaching and retracting curves, which is related to viscous properties of the cell. As the scan rate is increased this hysteresis increases to the point that a negative deflection of the cantilever occurs.

indentation, which is irreversible on the time scale of the experiment. Subsequent FD curves were collected at lower trigger values following the acquisition of the 200-nm curve. These curves overlapped with the 200-nm curve (results not shown), suggesting that the deformation is long-lived.

The premise for microelastic mapping using the AFM is based on the measurable variability in elasticity across the sample surface. AFM imaging of living MDCK cells shows the typical morphology of these cells (Hoh and Schoenenberger, 1994). Several distinct regions of the cell can be identified from the height signal image (Fig. 7 *A*). The large structure in the center of the cells appears to be the nucleus. Cell boundaries can be seen in some of these images, but are more distinct in the error signal image (not shown). Fig. 7 *B* shows six FD curves obtained on different parts of the MDCK cells' monolayer shown in Fig. 7 *A*. The curves collected over the nucleus differed markedly from those two curves over the cell boundaries and the ones over the cell body.

FIEL Mapping of MDCK Cells

FIEL mapping of monolayers of living MDCK cells produces images with features that are independent of topography and trigger height images (Fig. 8). The topographic image is constructed from the force volume at the lowest detectable cantilever deflection (Fig. 8 *A*2 and *B*2), while

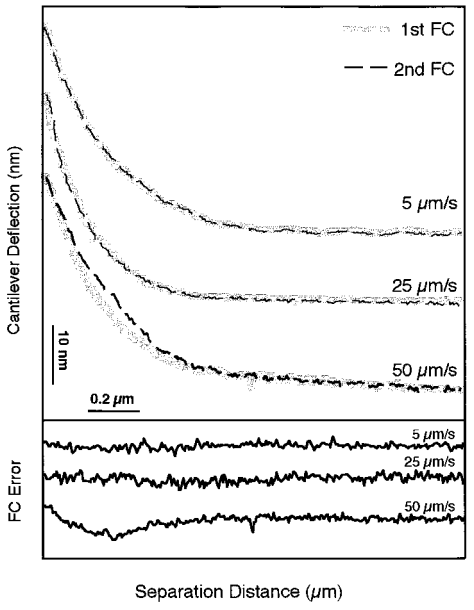

FIGURE 5 Consecutive pairs of force curves taken on the same position on an MDCK monolayer, with different scan rates. The lower box shows the result of subtraction of first curve from second curve within each pair. For the 4 and 25 μm/s pairs, the two force curves are identical, while there is a clear deviation between the 50 μm/s force curve pairs.

the trigger height image is the *Z* piezo position at the cantilever trigger (Fig. 8 *A*3 and *B*3). The convention for topographic AFM imaging is that the light areas are higher than the dark areas. For FIEL mapping we have adopted the convention that light areas are less stiff than dark ones. The

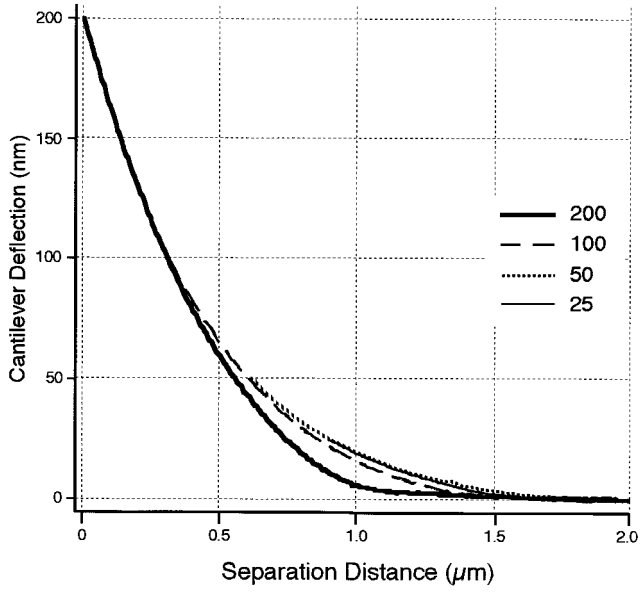

FIGURE 6 Effect of increasing indentation depth of the monolayer by the tip. Several FD curves with different trigger values taken on the same spot are aligned by their maximum deflections (triggers). At smaller indentations the curves overlap, while at the larger indentation the curves do not overlap, indicating the presence of a deformation that does not reverse on the time scale of the experiment.

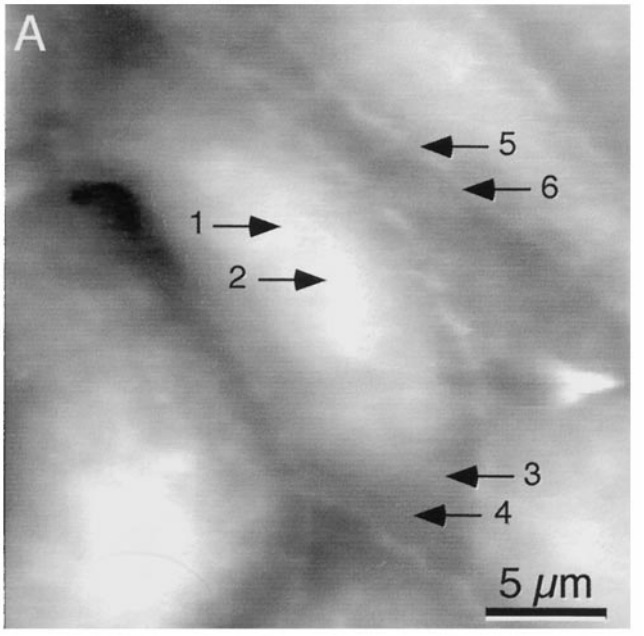

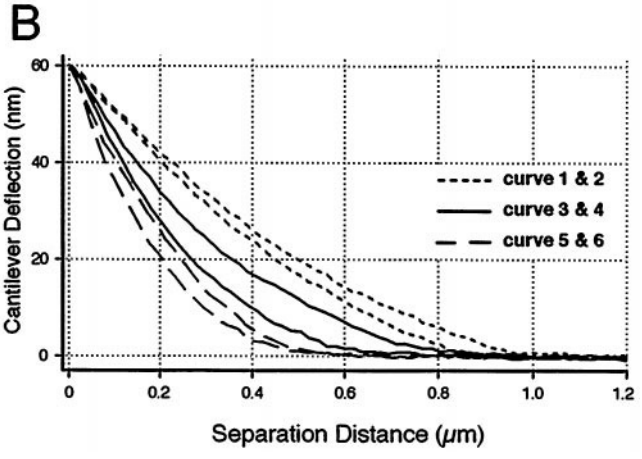

FIGURE 7 Variation of stiffness across the surface of MDCK cells, measured by individual FD curves. (*A*) The height image shows the surface morphology of MDCK cells. The nucleus is very prominent in this image, being the highest point on the cell. (*B*) Sample of six FD curves taken on different position on the MDCK monolayer shown in (*A*). The arrows denote positions where the curves were collected.

centers of the cells are relatively "soft," while the cell-cell boundaries are relatively stiff. Although the general morphology of the cells is the same in topographic and FIEL maps, cross-sections through the images show significant differences (Fig. 8, *bottom*) and occasional contrast inversion (*arrow* in Fig. 8, *B*1 and *B*3). Therefore, the FIEL maps show features that have a different basis for contrast. Furthermore, the theoretical basis for FIEL predicts that these maps are internally quantitative without calibration of the cantilever spring constant. However, in order to compare FIEL maps collected with different cantilevers the spring constants must be calibrated and the trigger force must be

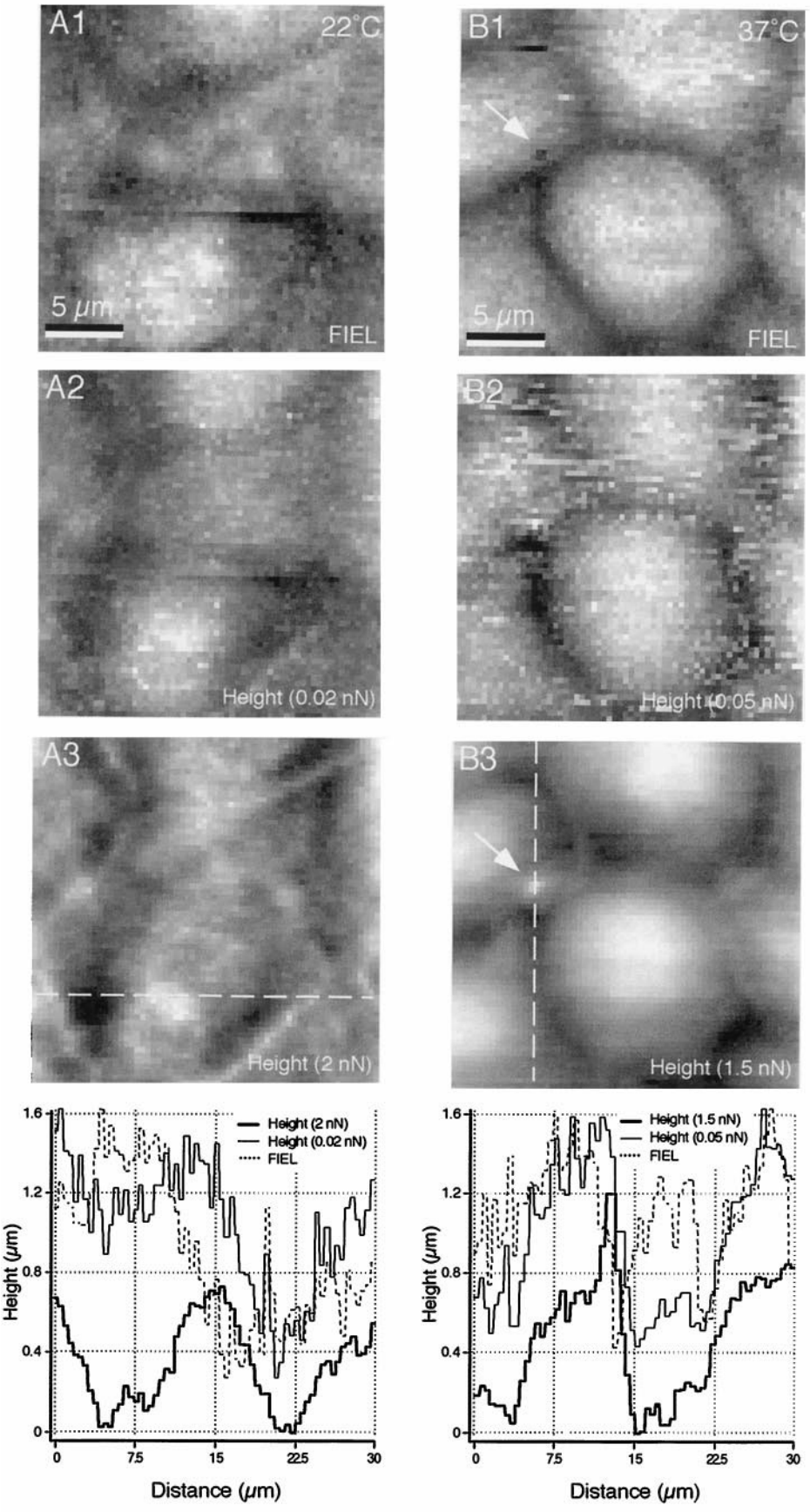

FIGURE 8 FIEL maps of monolayers of living MDCK cells at (*A*1) 22°C and (*B*1) 37°C, and the corresponding topographic maps of the MDCK monolayer reconstructed at (*A*2 and *B*2) low and (*A*3 and *B*3) high loading forces. The range of gray scales in the FIEL maps is from relatively stiff (*dark*) to soft (*light*). Cross-sections through the topographic maps and the FIEL maps show variations across the surface, with occasional contrast inversion (*arrows*).

set to the same value for each map. Note that the maps presented here have not been scaled for tip geometry and thus are not linear.

At higher resolutions, FIEL maps often show a great deal of intriguing fine detail (Fig. 9). One of the most readily identifiable structures seen in some FIEL maps is the nucleus, which is demarked by a change in stiffness between it and the cell body. Curiously, a structure that follows the nuclear boundary, or is the nuclear boundary itself, often appears to have a relatively low stiffness compared to the nucleus and cytoplasm (Figs. 9 *A* and 11 *D*2). Such contrast appears to be slightly peri-nuclear and may arise from the organization of cytoskeletal components in the cytosol and around the nucleus. Contrast in stiffness at the cell boundaries is clearly seen in Fig. 8, and is highlighted at higher magnification in Fig. 9 *B*. Similar to the region around the nucleus there is often an unexpected pattern of stiffness, in which the boundary between the two cells is a stiff band that is divided by an irregular less stiff "line" (denoted by the white arrows). The junctional complexes, in addition to their various physiological functions, impart mechanical strength to epithelial sheets (Pasdar and Li, 1993; Wacker et al., 1992; Armitage et al., 1994). One might speculate that the discontinuous appearance along the length of this cell boundary line is due to variable distribution of cell junctions along the cell boundaries. Fig. 9 *C* shows a less frequent observation, in which average stiffness varied greatly between several neighboring cells in a MDCK monolayer. More often, MDCK cells show comparable differences in stiffness over their various parts. The reason for such large difference in contrast is not clear, although it may suggest a more general difference in the states of the cells.

The question of which of the features in an image are real and which are the result of a spurious behavior of the cantilever during an individual FD curve is addressed by repeated imaging over the same area (Fig. 10). The FIEL maps are extremely consistent, with many detailed features persisting over the time scale of many hours. The details that do not persist may have been the result of an artifact or may simply have changed over time. Better understanding of this issue will come with more experience in FIEL mapping of cells. Furthermore, the persistent details provide an estimate of the lateral resolution of FIEL mapping. Several features on the order of 200 nm are stable, suggesting that the current resolution of FIEL mapping is comparable to that of optical microscopy. The image series in Fig. 10 also shows the temporal resolution of FIEL mapping. For a 64×64 image of MDCK cells the typical acquisition time is on the order of 2 h. This is limited by the rate of collecting individual FD curves such that the viscous contribution is minimized. While this time can easily be reduced by half through modifications in the data acquisition software, further improvements will be incremental with the current analytical approach and experimental tools. At present the most straightforward way to increase the temporal resolution is to limit the number of FD curves collected by carefully defining the region of interest, in which case the limit is ~0.5 s for a single FD curve.

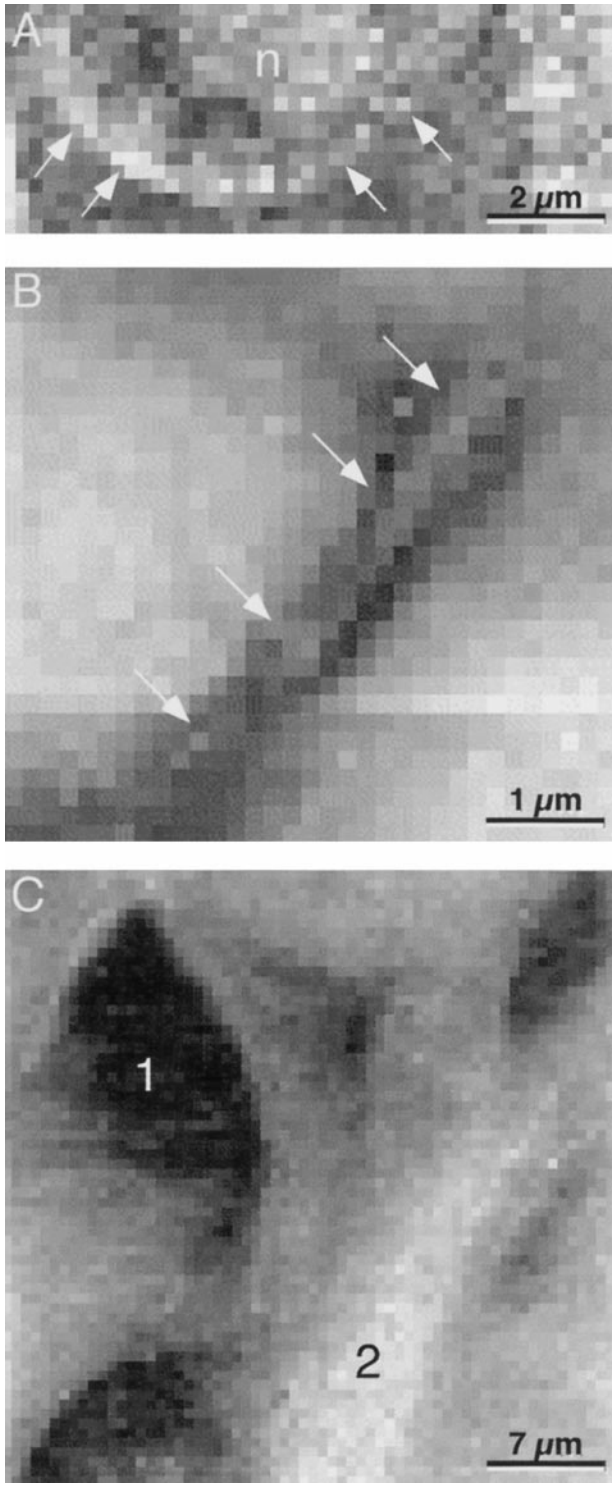

FIGURE 9 Unexpected features in FIEL maps of MDCK cells. (*A*) High magnification of the boundary of a nucleus show a region that is softer than the cytoplasm and nucleoplasm (*arrows*). (*B*) A soft transition, bounded by stiff regions, is also seen in high magnification maps of cell-cell boundaries. (*C*) Occasionally there is a very large variations in elastic properties of different cells within a monolayer (compare cells marked 1 and 2).

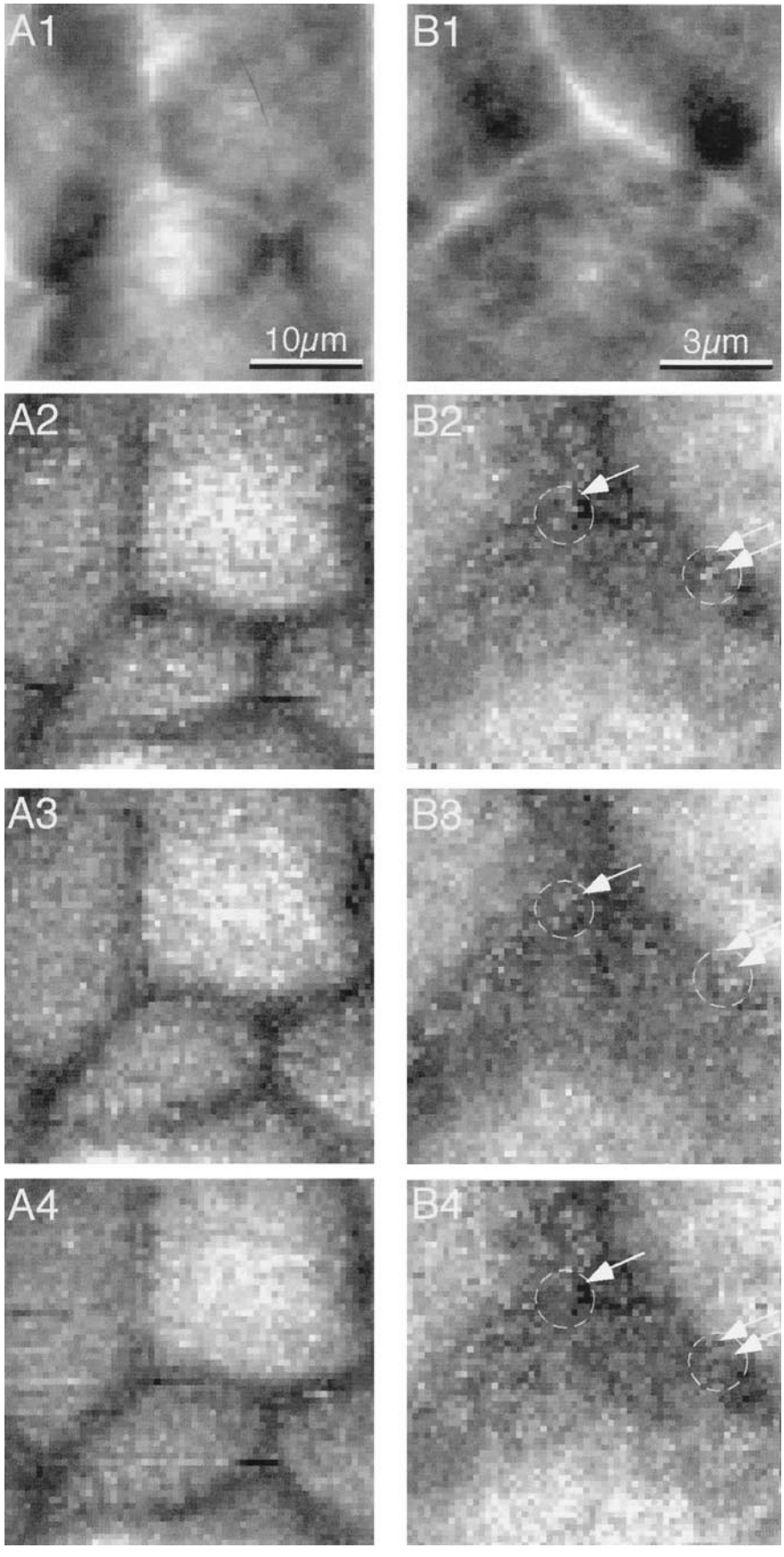

FIGURE 10 Repeated FIEL mapping on MDCK monolayers at (*A*) 30 × 30 μm and (*B*) 10 × 10 μm. The first two images correspond to the topography (*A*1, *B*1), and the three consecutive FIEL maps (~2 h for each map) for each monolayer are shown in the column below the topography. All volumes are 64 × 64 × 64. The 30 × 30 μm and 10 × 10 μm scans are extremely reproducible over the time scale of several hours. Many small features appear in sequential maps (*arrows* and *double arrows*), but change in the third map. That they remain after two hours, but change after four, suggests that these features reflect a real part of the cell. Very high resolution maps (1 × 1 μm) are very noisy and have no obvious morphological features (not shown).

The individual FD curves suggest that using the smallest deformations possible appears to give the most quantitative results. However, the contrast in the FIEL maps depends on the applied force, and hence on the degree of deformation (Fig. 11). At higher indenting forces new structures appear, while others become more well defined. This suggests, not unexpectedly, that as the indentation depth increases the sample represented in the individual FD curves, the sample becomes increasingly anisotropic in the *Z* direction.

It should be noted that currently we do not have independent means of establishing the cellular or molecular origin of many of the morphological details seen in the FIEL maps. However, based on immunofluorescence microscopy studies that show distinct localization patterns for several cytoskeletal components (Pasdar and Li, 1993; Dugina et al., 1995; Huotari et al., 1996), and general morphological features of these cells, we have assigned identities to some of the features seen in the FIEL maps. With a new imaging technology such as the AFM, caution is also in order. It is likely that artifacts will emerge that have not yet been identified, such as complex geometric effects of tip sample interactions.

The effect of viscosity can be seen in FIEL maps collected at different temperatures (Fig. 8) and scan rates (Fig

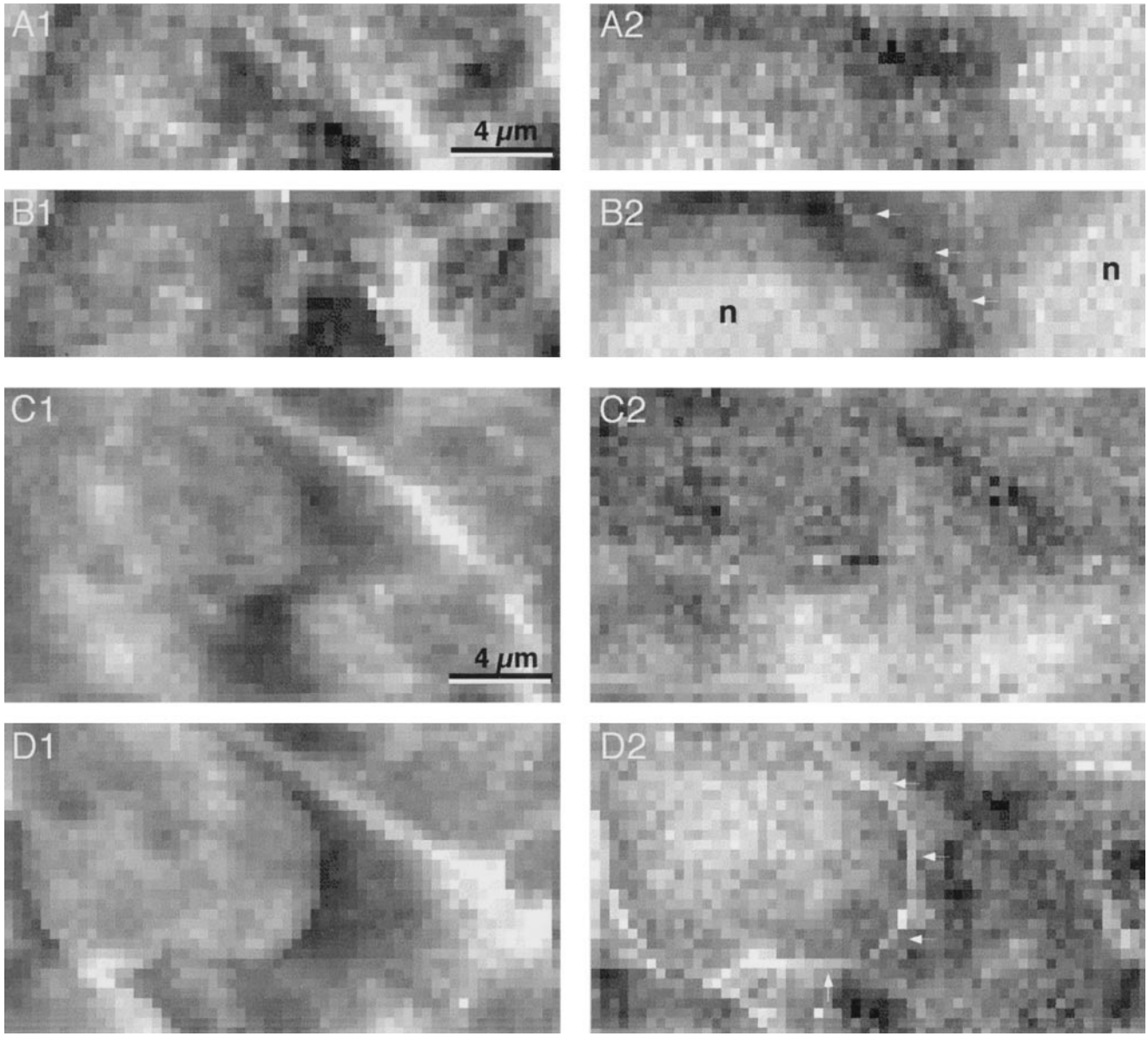

FIGURE 11 Effect of indentation depth on contrast in FIEL maps of MDCK cells. (*A*1) shows topography and the corresponding FIEL map (*A*2) of an MDCK monolayer collected at a 1.5 nN trigger, while (*B*1) shows topography and FIEL map (*B*2) of the same monolayer collected at a 3 nN trigger. An increase in contrast of both (*B*1) and (*B*2) can be seen as a result of increasing indentation depths, and the larger indentations show more detailed structures such as the soft cell-cell boundary (*arrows*). Similarly, (*C*1) shows topography and a FIEL map (*C*2) at a 1.5-nN trigger, and a consecutive scan of the same monolayer, topography (*D*1) and FIEL map (*D*2), at a 6-nN trigger. Again, more details are seen in high-force maps, including a soft region that appears to be peri-nuclear (*white arrows*).

12). At 37°C the contrast is more pronounced than at room temperature. This is consistent with the analysis of the FT and FD curves, which predicts that viscous contributions would increase at lower temperatures. The viscous contribution is also seen in a comparison of FIEL maps collected at different scan rates. These show greater contrast in the slow scan rate maps (Fig. 12 *A*; 8 μm/s) than the fast rate ones (Fig. 12 *B*; 80 μm/s). The time dependence of viscosity makes cells appear stiffer at faster scan rates. Thus the faster scan rate FIEL maps should have less contrast. In principle, disregarding the imaging fluid's hydrodynamics, a scan rate that approaches infinity should produce a close to solid contact point and a perfectly "flat" FIEL map with no contrast.

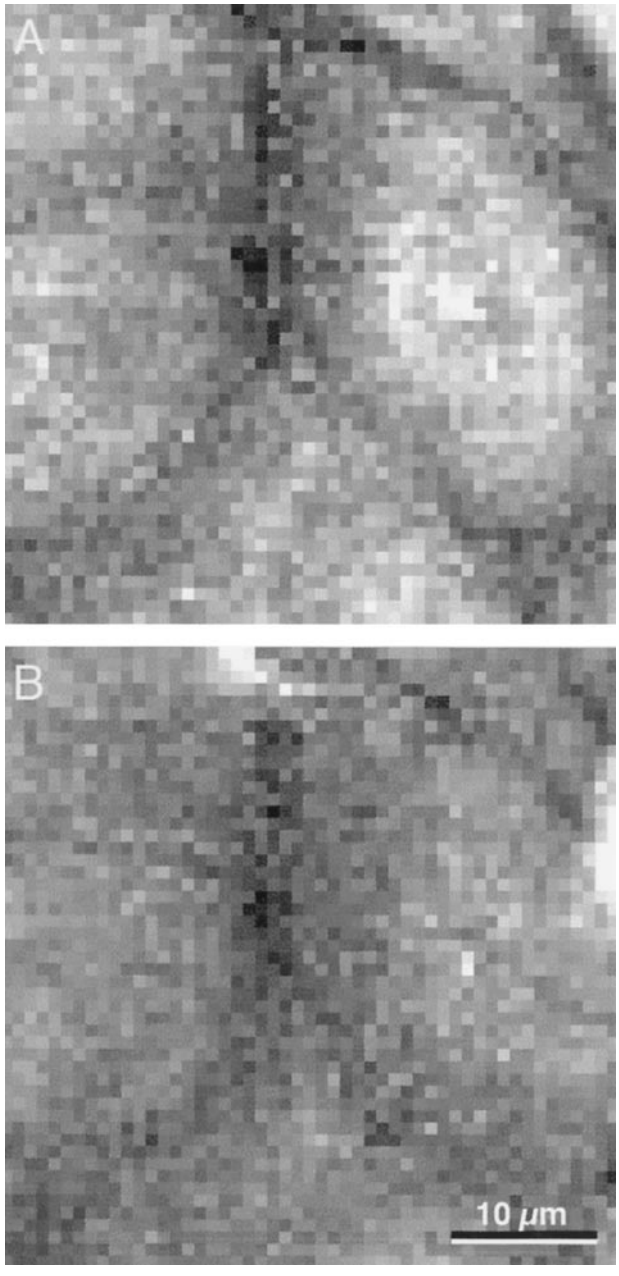

FIGURE 12 FIEL maps of MDCK cells collected at scan rates of (*A*) 8 μm/s and (*B*) 80 μm/s. In relationship to the FT curves shown in Fig. 1 *C*, measurements at high scan rates coincide with the early part of the period [D-E], while the slow scan rates are closer to [E]. Therefore, the fast scan rate image has a significant viscous contribution, and appears flatter than the slow scan rate image.

Limitations of FIEL mapping

There are a number of obvious limitations and concerns with FIEL mapping on living cells. Cells move and change in response to mechanical stimuli, and thus the FD curves may contain active responses that do not reflect viscoelasticity. Cells are also highly anisotropic, and so the FIEL maps can not be absolutely quantitative. We defined elasticity as the time-independent component of the indentation measurements and viscosity as the time-dependent component. While this is not strictly correct, it is the only practical definition that could be currently used. However, our main goal is to visualize spatial and temporal *changes* in mechanical properties of living cells. The extent to which FIEL mapping will be useful for this, or which the concerns discussed above will limit its use, can only be determined with further experimentation. FIEL is also limited by current AFM designs. One particular problem that must be addressed is the relationship between the position of the tip (or shape of the cantilever) and the endslope measurement used in the optical lever detection system.

CONCLUSIONS

The spatial and temporal changes of the mechanical properties of living cells reflect complex underlying physiological processes. We have developed an experimental approach, using atomic force microscopy, called FIEL mapping, to produce robust maps of relative elasticity. FIEL mapping has the advantage over previous approaches of being essentially independent of the contact point and the cantilever spring constant. By collecting force-distance curves on a time scale where viscous contributions are small, the forces measured are dominated by the elastic properties of the sample. FIEL maps on MDCK cells show that the elasticity is uncoupled from the topography and reveal a number of unexpected features. These results present a mode of high-resolution visualization useful for living biological materials in which the contrast is based on the mechanical properties of the sample.

We thank Dr. Elias Zerhouni for the use of his AFM, Dr. Frank Yin for helpful discussions, and D. Papageorgiou for help with the manuscript.

This work was supported by grants from the Muscular Dystrophy Association and the Whitaker Foundation for Biomedical Engineering (to J.H.H.). William F. Heinz was supported in part by National Institutes of Health Predoctoral Training Grant T32 GM-08043.

REFERENCES

Armitage, W. J., B. K. Juss, and D. L. Easty. 1994. Response of epithelial (MDCK) cell junctions to calcium removal and osmotic stress is influenced by temperature. *Cryobiology.* 31:453–460.

Ashkin, A., and J. M. Dziedzic. 1989. Internal cell manipulation using infrared laser traps. *Proc. Natl. Acad. Sci. USA.* 86:7914–7918.

Balkovetz, D. F., A. L. Pollack, and K. E. Mostov. 1997. Hepatocyte growth factor alters the polarity of Madin-Darby canine kidney cell monolayers. *J. Biol. Chem.* 272:3471–3471.

Bereiter-Hahn, J., K. Ilonka, H. Luers, and M. Voth. 1995. Mechanical basis of cell shape: investigations with the scanning acoustic microscope. *Biochem. Cell Biol.* 73:337–348.

Binnig, G., C. F. Quate, and C. Gerber. 1986. Atomic force microscope. *Phys. Rev. Lett.* 56:930–933.

Bottomley, L. A., J. E. Coury, and P. N. First. 1996. Scanning probe microscopy. *Anal. Chem.* 68:185R–230R.

Briscoe, B. J., and S. K. Sebastian. 1993. An analysis of the "durometer" indentation. *Rubber Chemistry and Technology.* 66:827–836.

Butt, H.-J., M. Jaschke, and W. A. Ducker. 1995. Measuring surface forces in aqueous electrolyte solution with the atomic force microscope. *Bioelectrochem. Bioenerg.* 38:191–201.

Butt, H. J., E. K. Wolf, S. A. C. Gould, and P. K. Hansma. 1991. Imaging cells with the atomic force microscope. *J. Struct. Biol.* 105:54–61.

Casa, F., M. Fenzi, and L. Tontodonati. 1995. Study of hardness drift: a method for investigating the viscous behavior of cured rubber. *Polymer Testing.* 14:355–367.

D'Costa, N. P, and J. H. Hoh. 1995. Calibration of optical lever sensitivity for atomic force microscopy. *Rev. Sci. Instr.* 66:5096–5097.

Ducker, W. A., T. J. Senden, and R. A. Pashley. 1992. Measurement of forces in liquids using a force microscope. *Langmuir.* 8:1831–1836.

Dugina, V. B., A. Y. Alexandrova, K. Lane, E. Bulanova, and J. M. Vasiliev. 1995. The role of the microtubular system in the cell response to HGF/SF. *J. Cell Sci.* 108:1659–1667.

Fritz, M., M. Radmacher, N. Peterson, and H. E. Gaub. 1994. Visualization and identification of intracellular structures by force modulation microscopy and drug induced degradation. *J. Vac. Sci. Technol. B.* 12: 1526–1529.

Fung, Y. C. 1988. Biomechanics: Mechanical Properties of Living Tissues. Springer-Verlag, New York.

Goldmann, W. H., and R. M. Ezzell. 1996. Viscoelasticity in wild-type and vinculin-deficient (5.51) mouse F9 embryonic carcinoma cells examined by atomic force microscopy and rheology. *Exp. Cell Res.* 226:234–237.

Hansma, H. G., and J. H. Hoh. 1994. Biomolecular imaging with the atomic force microscope. *Annu. Rev. Biophys. Chem.* 23:115–139.

Haydon, P. G., R. Lartius, V. Parpura, and S. P. Marchese-Ragona. 1996. Membrane deformation of living glial cells using atomic force microscopy. *J. Microsc.* 182:114–120.

Henderson, E. 1994. Imaging of living cells by atomic force microscopy. *Prog. Surface Sci.* 46:39–60.

Henderson, E., P. G. Haydon, and D. S. Sakaguchi. 1992. Actin filament dynamics in living glial cells imaged by atomic force microscopy. *Science.* 257:1944–1946.

Hertz, H. 1881. Über den kontakt elastischer körper. *J. Reine Angew. Mathematik.* 92:156.

Hoh, J. H., and A. Engel. 1993. Friction effects in force curves. *Langmuir.* 9:3310–3312.

Hoh, J. H., and C.-A. Schoenenberger. 1994. Surface morphology and mechanical properties of MDCK monolayers by atomic force microscopy. *J. Cell Sci.* 107:1105–1114.

Huotari, V., J. Vääräniemi, V.-P. Lehto, and S. Eskelinen. 1996. Regulation of the disassembly/assembly of the membrane skeleton in Madin-Darby canine kidney cells. *J. Cell. Physiol.* 167:121–130.

Ingber, D. E. 1993. Cellular tensegrity: defining new roles of biological design that governs the cytoskeleton. *J. Cell Sci.* 104:613–627.

Ingber, D. E., L. Dike, L. Hansen, S. Karp, H. Liley, A. Maniotis, H. McNamee, D. Mooney, G. Plopper, J. Sims, and N. Wang. 1994. Cellular tensegrity: exploring how mechanical changes in the cytoskeleton regulate cell growth, migration, and tissue pattern during morphogenesis. *Int. Rev. Cytol.* 150:173–224.

Ingber, D. E., and J. Folkman. 1989. Tension and compression as basic determinants of cell form and function: Utilization of a cellular tensegrity mechanism. *In* Cell Shape: Determinants Regulation and Regulatory Role. W. D. Stein and F. Bronner, editors. Academic Press, Orlando, Florida. 1–32.

Ingber, D. E., and J. D. Jamieson. 1985. Cells as tensegrity structures: Architectural regulation of hystodifferentiation by physical forces transduced over basement membrane. *In* Gene Expression during Normal and Malignant Differentiation. L. C. Anderson, C. G. Gahmberg, and P. Ekblom, editors. Academic Press, London, 13–32.

Ingber, D. E., D. Prusty, Z. Sun, H. Betensky, and N. Wang. 1995. Cell shape, cytoskeletal mechanics, and cell cycle control in angiogenesis. *J. Biomechanics.* 28:1471–1484.

Johnson, K. L. 1985. Contact Mechanics. Cambridge University Press, Cambridge.

Kasas, S., N. H. Thomson, B. L. Smith, P. K. Hansma, J. Miklossy, and H. G. Hansma. 1997. Biological applications of the AFM: from single molecules to organs. *Int. J. Imaging Systems and Technology.*8:151–161.

Laney, D. E., R. A. Garcia, S. M. Parsons, and H. G. Hansma. 1997. Changes in the elastic properties of cholinergic synaptic vesicles as measured by atomic force microscopy. *Biophys. J.* 72:806–813.

Li, M., J. Ageller, D. A. Farson, C. Hatier, J. Hassell, and M. J. Bissell. 1987. Influence of a reconstituted basement membrane and its components on casein gene expression and secretion in mouse mammary epithelial cells. *Proc. Natl. Acad. Sci. USA.* 84:136–140.

Luers, H., K. Hillmann, J. Litniewski, and J. Berciter. 1991. Acoustic microscopy of cultured cells: distribution of forces and cytoskeletal elements. *Cell Biophys.* 18:279–293.

Maniotis, A. J., C. S. Chen, and D. E. Ingber. 1997. Demonstration of mechanical connections between integrins, cytoskeletal filaments, and nucleoplasm that stabilize nuclear structure. *Proc. Natl. Acad. Sci. USA.* 94:849–854.

Matlin, K. S., and M. J. Caplan. 1992. Epithelial cell structure and polarity. *In* The Kidney: Physiology and Pathophysiology. D. W. Seldin and G. Giebisch, editors. Raven Press, New York. 447–473.

Mitchison, T. J. 1995. Evolution of a dynamic cytoskeleton. *Phil. Trans. R. Soc. Lond. B.* 349:299–304.

Mooney, D., L. Hansen, J. Vacanti, R. Langer, S. A. Farner, and D. Ingber. 1992. Switching from differentiation to growth in hepatocytes: control by extracellular matrix. *J. Cell Physiol.* 151:497–505.

Pasdar, M., and Z. Li. 1993. Disorganization of microfilaments and intermediate filaments interferes with the assembly and stability of desmosomes in MDCK epithelial cells. *Cell Motil. Cytoskeleton.* 26:163–180.

Peterson, N. O., W. B. McConnaughey, and E. L. Elson. 1982. Dependence of locally measured cellular deformability on position on the cell, temperature, and cytochalasin B. *Proc. Natl. Acad. Sci. USA.* 79: 5327–5331.

Putman, C. A., K. O. van der Werf, B. G. de Grooth, N. F. van Hulst, and J. Greve. 1994. Viscoelasticity of living cells allows high resolution imaging by tapping mode atomic force microscopy. *Biophys. J.* 67: 1749–1753.

Radmacher, M., J. P. Cleveland, M. Fritz, H. G. Hansma, and P. K. Hansma. 1994. Mapping interaction forces with the atomic force microscope. *Biophys. J.* 66:2159–2165.

Radmacher, M., M. Fritz, and P. K. Hansma. 1995. Imaging soft samples with the atomic force microscope: gelatin in water and propanol. *Biophys. J.* 69:264–278.

Radmacher, M., M. Fritz, C. Racher, J. P. Cleveland, and P. K. Hansma. 1996. Measuring the viscoelastic properties of human platelets with the atomic force microscope. *Biophys. J.* 70:556–567.

Schaus, S. S., and E. R. Henderson. 1997. Cell viability and probe-cell membrane interactions of XR1 glial cells imaged by atomic force microscopy. *Biophys. J.* 73:1205–1214.

Schoenenberger, C.-A., and J. H. Hoh. 1994. Slow cellular dynamics in MDCK and R5 cells monitored by time-lapse atomic force microscopy. *Biophys. J.* 67:929–936.

Shao, J., and R. M. Hochmuth. 1996. Micropipette suction for measuring piconewton forces of adhesion and tether formation from neutrophil membranes. *Biophys. J.* 71:2892–2901.

Shroff, S. G., D. R. Saner, and R. Lal. 1995. Dynamic micromechanical properties of cultured rat atrial myocytes measured by atomic force microscopy. *Am. J. Physiol.* 269:C286–C289.

Singhvi, R., A. Kumar, G. Lopez, G. N. Stephanopoulos, D. I. C. Wang, G. M. Whitesides, and D. E. Ingber. 1994. Engineering cell shape and function. *Science.* 264:696–698.

Svoboda, K., C. F. Schmidt, D. Branton, and S. M. Block. 1992. Conformation and elasticity of the isolated red blood cell membrane skeleton. *Biophys. J.* 63:784–793.

Tao, N. J., S. M. Lindsay, and S. Lees. 1992. Measuring the microelastic properties of biological material. *Biophys. J.* 63:1165–1169.

Valberg, P. A., and H. A. Feldman. 1987. Magnetic particle motions within living cells. *Biophys. J.* 52:551–561.

Wacker, I. U., J. E. Rickard, I. R. De Mey, and T. E. Kreis. 1992. Accumulation of a microtubule-binding protein, pp170, at desmosomal plaques. *J. Cell Biol.* 117:813–824.

Wang, N., and D. E. Ingber. 1994. Control of cytoskeletal mechanics by extracellular matrix, cell shape, and mechanical tension. *Biophys. J.* 66:2181–2189.

Weisenhorn, A. L., P. Maivald, H. J. Butt, and P. K. Hansma. 1992. Measuring adhesion, attraction, and repulsion between surfaces in liquids with an atomic force microscope. *Phys. Rev. B (Condensed Matter).* 45:11226–11232.

Young, A., and E. Evans. 1989. Cortical shell-liquid core model for passive low of liquid-like spherical cells into micropipettes. *Biophys. J.* 56: 139–149.

Zahalak, G. I., W. B. McConnaughey, and E. L. Elson. 1990. Determination of cellular mechanical properties by cell poking, with an application to leukocytes. *J. Biomechanical Eng.* 112:283–294.

Zeman, K., H. Engeljhardt, and E. Sackmann. 1990. Bending undulations and elasticity of the erythrocyte membrane: effect of cell shape and membrane organization. *Eur. Biophys. J.* 18:203–219.

Zheng, J., P. Lamoureux, V. Santiago, T. Dennerll, R. E. Buxbaum, and S. R. Heidemann. 1991. Tensile regulation of axonal elongation and initiation. *J. Neurosci.* 11:1117–1125.

Zilker, A., H. Engelhardt, and E. Sackmann. 1987. Dynamic reflection interference contract (RIC) microscopy: a new method to study surface excitations of cells and to measure membrane bending elastic moduli. *J. Phys.* 48:2139–2151.